

Expanded View Figures

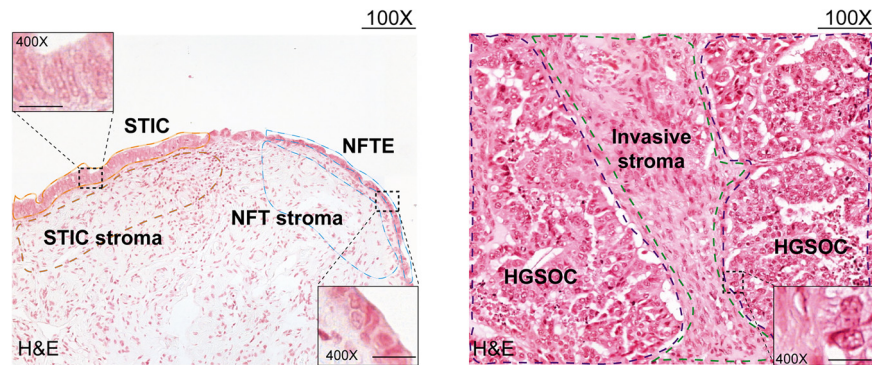


Figure EV1. Pathology-guided ultra-low input proteomics of HGSOC precursor lesions.

Representative H&E stains of normal fallopian tube epithelium (NFTE), serous tubal intraepithelial carcinoma (STIC), and invasive carcinoma (IC) and corresponding epithelial and stromal compartments. Scale bars: 100X: 100 μ m, 400X: 20 μ m.

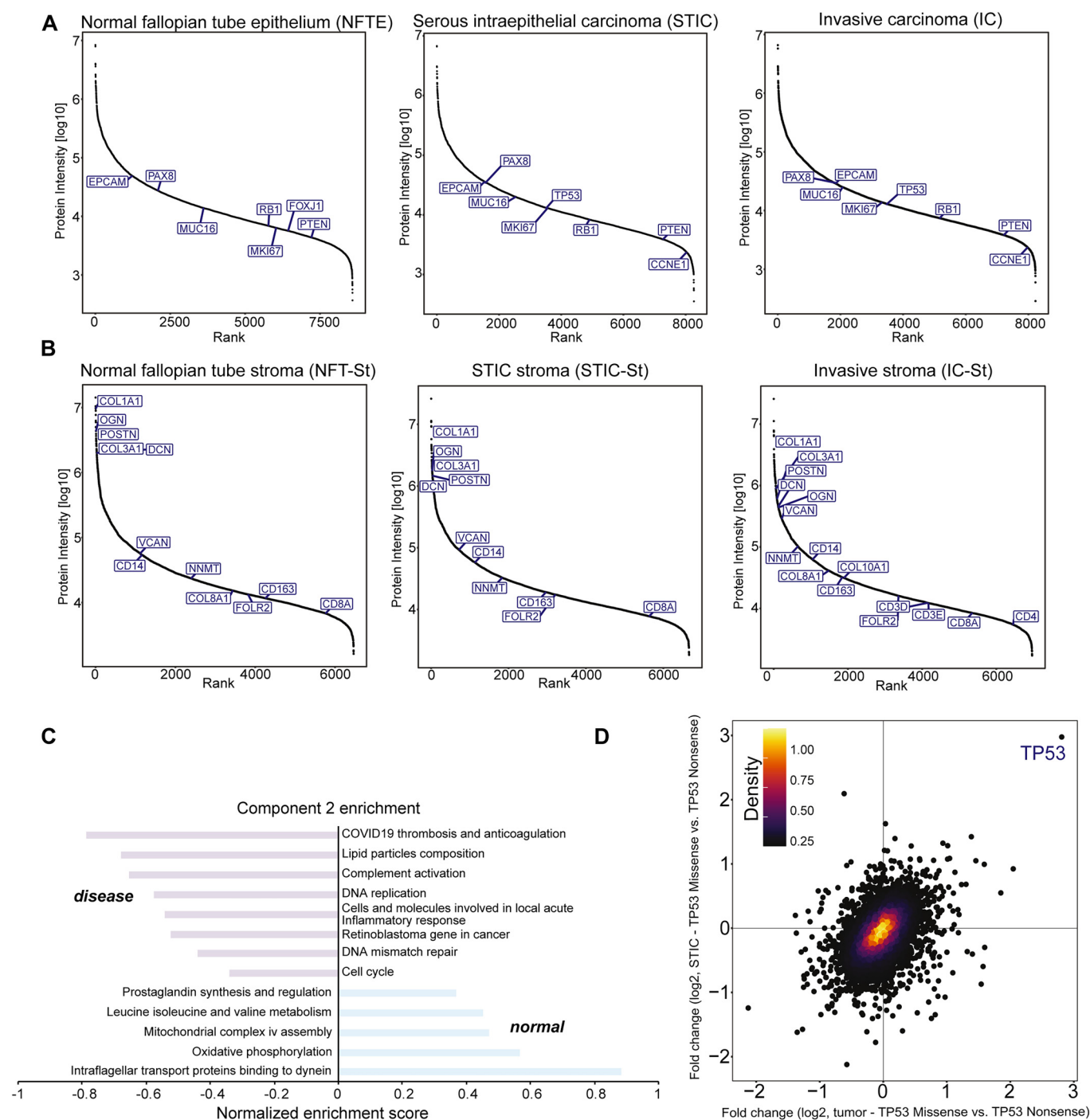
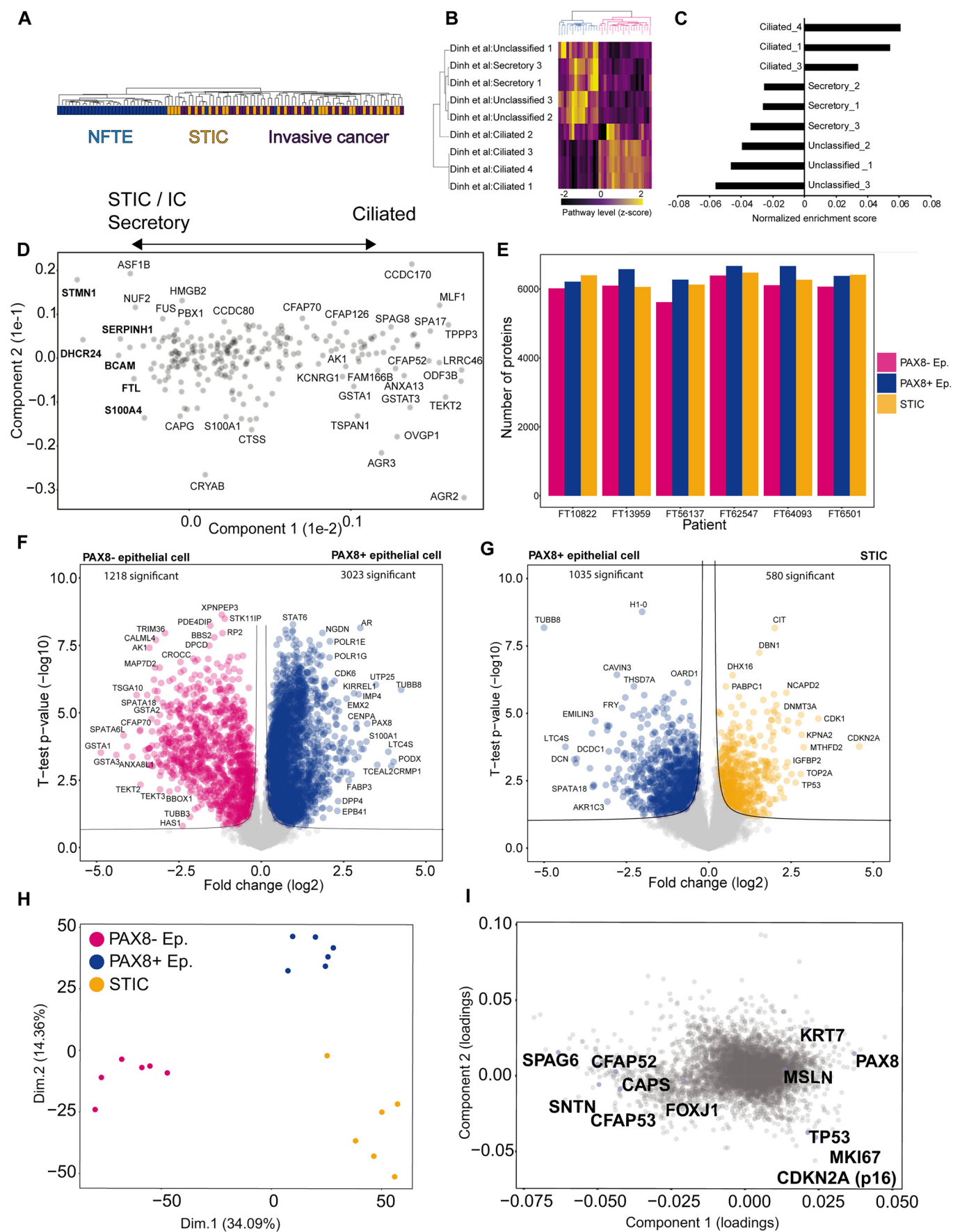


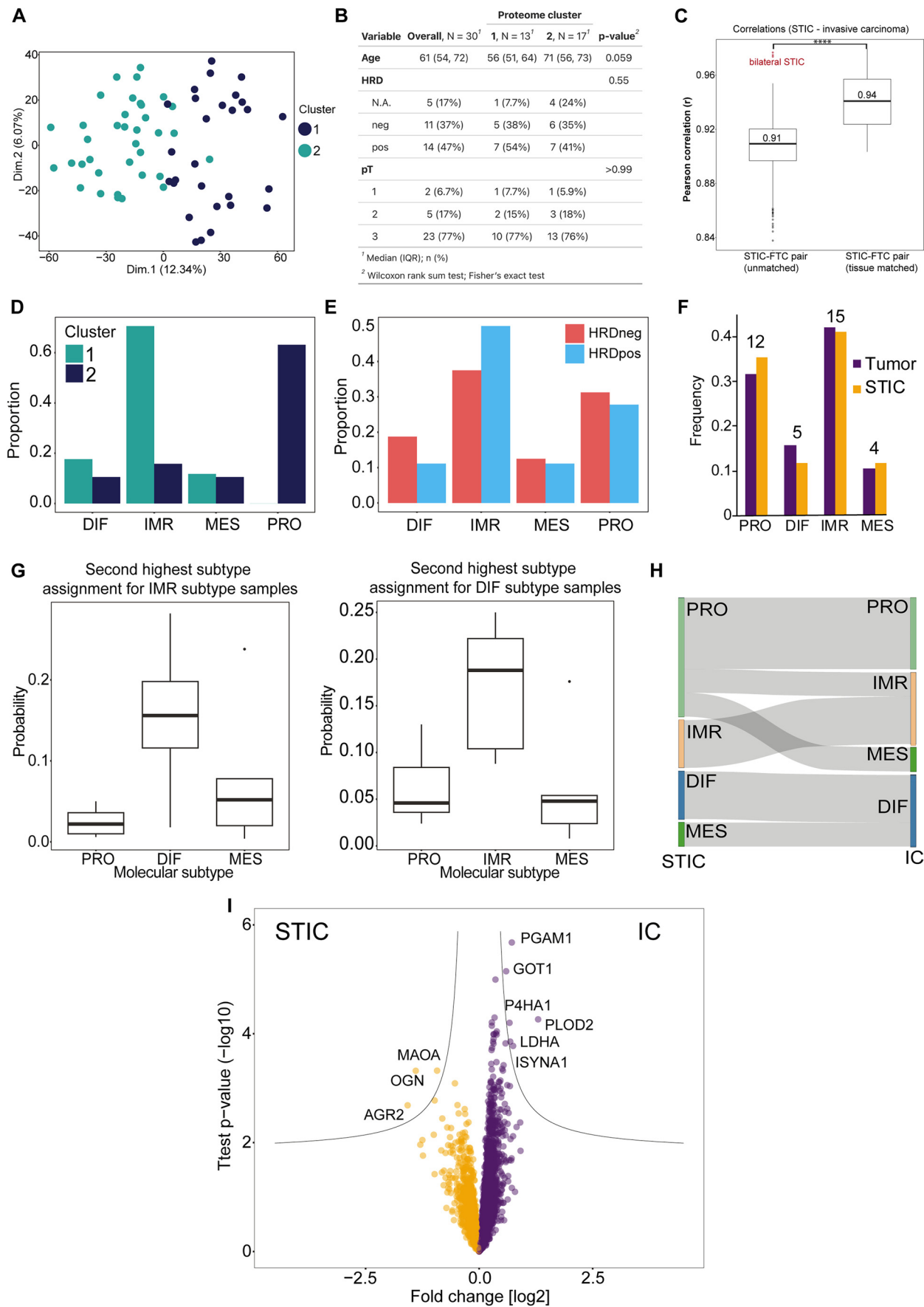
Figure EV2. Spatially resolved proteomes reflect disease-specific alterations at the bulk level depth.

(A, B) Dynamic range of median protein abundance for epithelial (A) and stromal (B) compartment samples. Known ovarian cancer-, cell type-, and stromal markers are highlighted. A minimum of 18 quantified values were required for each marker to be displayed. Proteins with 50% valid values for each group are shown. (C) Pathway enrichment analysis (Hallmarks) based on PC2 reveals differences between normal and disease compartments. Selected terms with a Benjamini-Hochberg FDR < 0.05 are shown. (D) Scatter plot of *t*-test results between p53 overexpression and p53 null mutation patients, indicating that p53 is the only differentially abundant protein between the two groups.



◀ **Figure EV3. Precursor lesions feature histological markers and cell-of-origin signatures.**

(A) Hierarchical tree showing the clustering pattern across regions (normal fallopian tube epithelium, STIC, and invasive fallopian tube carcinoma), revealing three epithelial samples that are atypical lesions based on proteome profiling. (B) Unsupervised hierarchical clustering of all normal fallopian tube epithelial samples based on cell type abundance scores. Cell type abundance scores were calculated based on the annotation matrix algorithm (Perseus) for all fallopian tube epithelial cell types identified by Dinh et al. Two main clusters of secretory and ciliated cell-enriched normal fallopian tube epithelium samples were identified. (C) Enriched cell type signatures along PC1, related to Fig. 3F. (D) PCA loadings related to Fig. 3F. Note that proteins on the left are higher in STIC, invasive carcinoma, and secretory-like epithelial cells, whereas proteins on the right are higher in ciliated epithelial cells. (E) Barplots showing the number of proteins identified in the PAX8 negative (dark pink), PAX8 positive (dark blue), and STIC (yellow) compartments across six patients. (F) Volcano plot of the pairwise proteomic comparison between PAX8 positive (dark blue, 6 samples) and PAX8 negative (dark pink, 6 samples) epithelial samples. Cell and functional markers with the highest abundance change and significance are highlighted (two-sided Student's *t*-test, FDR <0.05). (G) Volcano plot of pairwise proteomic comparison between STIC (yellow, 6 samples) and PAX8 positive (dark blue, six samples) samples. Cell and functional markers with the highest abundance change and significance are highlighted (two-sided Student's *t*-test, FDR <0.05). (H) PCA of all quantified proteins comparing STICs (yellow), secretory (dark blue), and ciliated cell (dark pink) samples. (I) PCA loadings show known secretory and ciliated markers. Related to panel (H).



◀ **Figure EV4. Refined molecular subtyping from spatial proteomics data.**

(A) Principal component analysis of STIC and invasive carcinoma samples corresponding to Fig. 3A. (B) Multivariate statistical analysis of patients in clusters 1 and 2. Note that cluster 2 samples showed a trend towards higher patient age at diagnosis ($p = 0.059$). (C) Boxplots showing proteomic correlations between STIC and invasive carcinoma samples between matched and unmatched samples, corresponding to inpatient and outpatient correlations. Boxplots define the range of the data (whiskers), 25th and 75th percentiles (box), and medians (solid line). (D) Molecular subtype assignment of cluster 1 and 2 samples based on the consensusOV algorithm(Chen et al, 2018). Only samples with a margin score of >0.2 were included for high classification confidence. (E) Molecular subtype assignment of HRD-positive and HRD-negative invasive cancer samples based on the consensusOV algorithm(Chen et al, 2018). (F) Frequency of molecular subtypes of STIC and IC proteomes. (G) Boxplots indicating the second-highest molecular subtype classification probabilities for samples with immunoreactive (left) and differentiated (right) subtype calls. Boxplots define the range of the data (whiskers), 25th and 75th percentiles (box), and medians (solid line). Number of samples per molecular subtype with margin score >0.2 : DIF - 5, PRO - 8, IMR - 5, MES - 2. (H) Sankey plot showing convergence or divergence of molecular subtypes for patient-matched STIC and invasive carcinoma pairs. (I) Volcano plot of pairwise proteomic comparison between STIC (yellow) and invasive fallopian tube carcinoma (violet) samples. Markers with the highest abundance change and significance are highlighted (two-sided Student's t-test, FDR <0.05). Number of samples per group: STIC - 35, IC - 31.

**Figure EV5. Mapping progressive ECM remodeling reveals stromal drug targets.**

(A) Volcano plot of pairwise proteomic comparison between IC stroma (purple, 29 samples) and NFT stroma (light blue, 31 samples) samples across different matrisome categories (collagens, ECM-affiliated, ECM glycoproteins, ECM regulators, proteoglycans, secreted factors). Markers with the highest abundance change and significance are highlighted (two-sided Student's *t*-test, FDR <0.05). (B, C) Boxplots of relative protein levels (group average, z-scored) for IC stroma (29 samples) (B) and NFT stroma (31 samples) (C)-associated features. Top-ranked protein features were identified by support vector machine classification, as shown in Fig. 5E. Boxplots define the range of the data (whiskers), 25th and 75th percentiles (box), and medians (solid line).

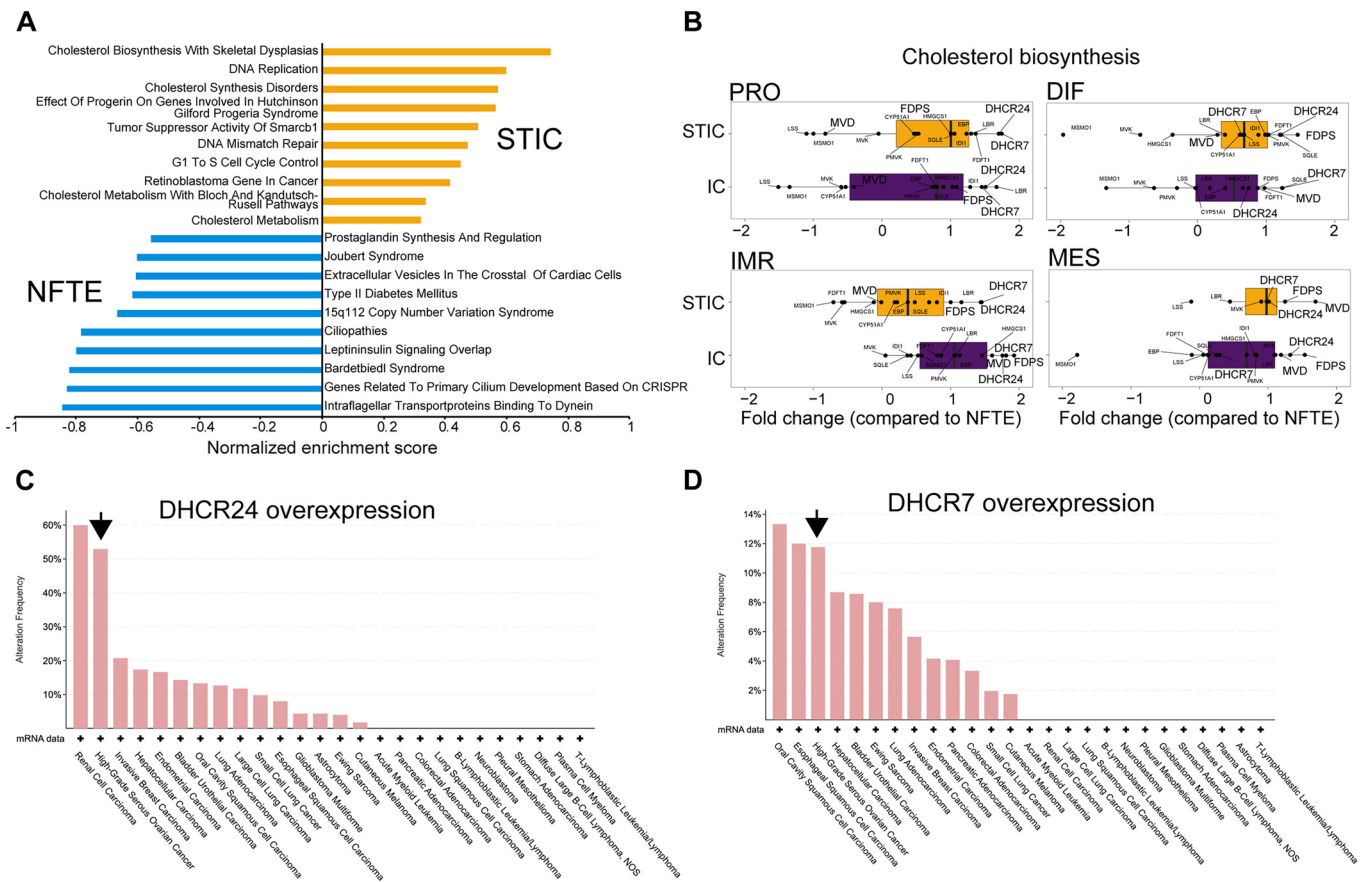




**Figure EV7. Cholesterol biosynthesis inhibition sensitizes ovarian cancer cells to carboplatin.**

(A–H) Dose-response curves (top left: AY9944 or simvastatin; bottom left: carboplatin) and dose-response matrices (right) for ES-2 (A, B), EFO-21 (C, D), OVCAR-8 (E, F), and OAW-42 (G, H) cells treated with AY9944 and carboplatin or simvastatin and carboplatin, respectively, alone or in combination. Experiments were performed in biological sextuplicate, each with $n = 3$ technical replicates.